THE DANIEL AND FLORENCE GUGGENHEIM MEMORIAL LECTURE

HOW TO IMPROVE THE PERFORMANCE OF TRANSPORT AIRCRAFT BY VARIATION OF WING ASPECT-RATIO AND TWIST

E. TRUCKENBRODT

HOW TO IMPROVE THE PERFORMANCE OF TRANSPORT AIRCRAFT BY VARIATION OF WING ASPECT-RATIO AND TWIST +

E. Truckenbrodt
Technical University of Munich

Abstract

The lecture deals with the influence of the wing aspect-ratio and twist on the induced drag of transport aircraft. Whereas the taper-ratio and the sweep of the wing are given, the aspect-ratio and twist are the two variable parameters. With respect to the critical transonic Mach-number a swept-forward wing has similar qualities as a swept-back wing, both at the same angle of sweep. The spanwise lift distribution will be discussed with regard to two aspects: elliptic lift distribution for the design lift coefficient and lift distribution for high lift coefficient in the vicinity of stalling. The investigation of induced drag leads to the result that a twisted swept-forward wing is equivalent to a twisted swept-back wing with an enlarged aspect-ratio.

+ 12th Daniel and Florence Guggenheim International Memorial Lecture

1. Introduction

At each Congress of the International Council of the Aeronautical Sciences (ICAS) the "Daniel and Florence Guggenheim International Memorial Lecture" should be presented on a subject of broad general interest by a lecturer of the host country. Whereas on the occasion of the 6th Congress, which took place here in Munich in 1968, Prof. A.W. Quick [10] gave a paper on aircraft propulsion, I should like to give today a contribution to the question of aircraft drag and thus to the question of economy of transport aircraft.

By means of a simple and clear study of parameters the influence of wing aspect-ratio and twist on the performance of a long range aircraft shall be demonstrated for tapered wings, see fig. 1. In this connection, besides of the

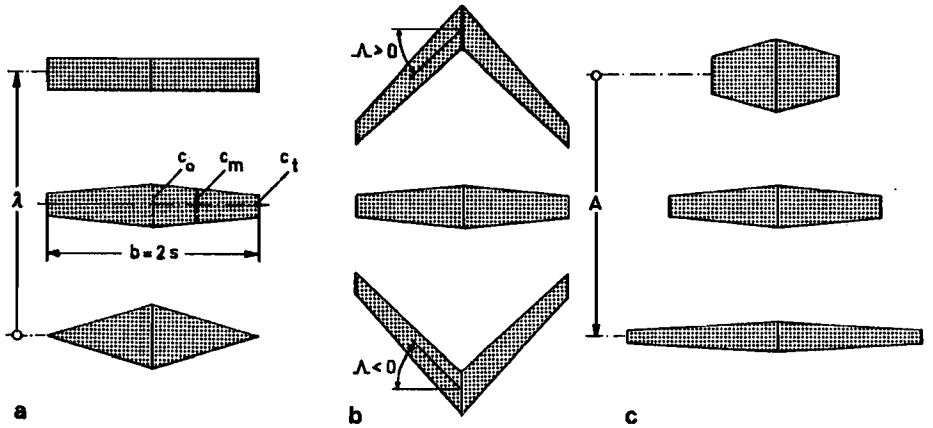

Figure 1 Geometric parameters of tapered wings
a) taper-ratio, $\lambda = c_t/c_o$; b) sweep, $\Lambda \lesseqgtr 0$; c) aspect-ratio, $A = b/c_m$

taper-ratio, it is above all the sweep that is particularly significant.

During the flight in the transonic regime the aerodynamics of aircraft is highly complex. Substantial improvements can be achieved by application of supercritical wing profiles in connection with sweep. These possibilities have been discussed on several occasions. They will not be subject of this lecture. It is assumed that the profiles have been optimized and that sweep is indispensable. Measurements show that the transonic aerodynamic characteristics of a swept-forward wing are not worse than those of an equivalent sweptback wing; they proved to be even better [15].

When the angle of incidence is large, flow separates on the wing first outboard in case of a swept-back wing, whereas in case of a swept-forward wing the opposite is true. With a swept-forward wing, the tips remain active well past the point where the inner portion of the wing stalls. With regard to this advantage, compared to the swept-back wing, the ailerons remain responsive even after the rest of the wing has stalled.

If minimal drag in cruising flight is postulated, and, in addition, if the wing should remain aerodynamically controllable at large angles of incidence, it appears that a twisted swept-forward wing, compared to a twisted swept-back wing, can be built with a smaller aspect-ratio.

My own work on the design and testing of the Ju 287 aircraft equipped with a swept-forward wing, see fig. 2a, as well as the HFB 320 aircraft of Hamburger Flugzeugbau, see fig. 2b, which also has a swept-forward wing, have given the impetous to the selection of the topic of my lecture.

The following survey covers the influence of the geometrical wing parameters given in fig. 1 on the induced drag. The interference of wing and fuselage will not be treated. Therefore, this study will essentially give general statements only.

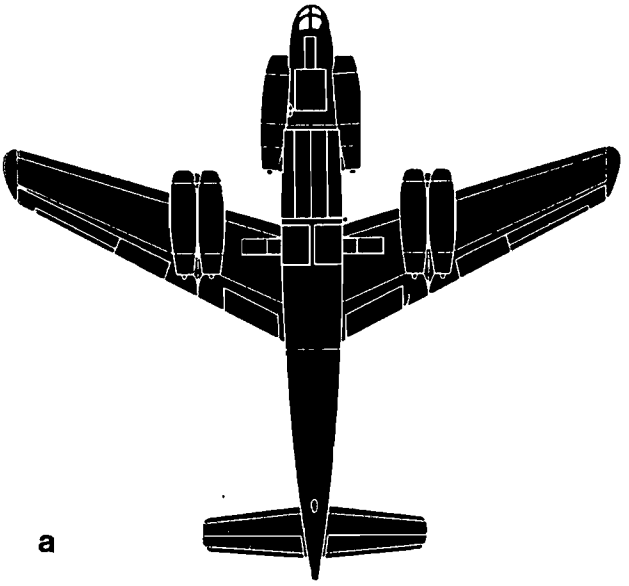

a

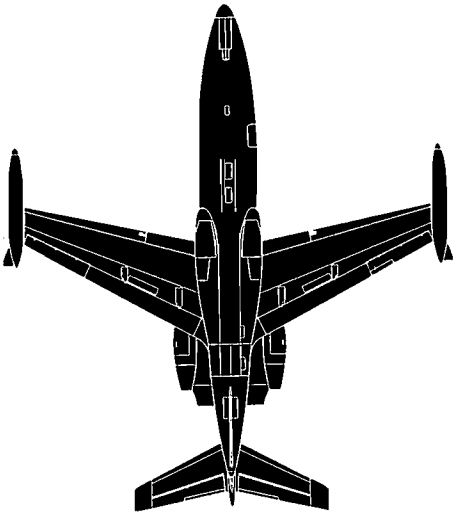

b

Figure 2 Airplanes with swept-forward wings
a) Junkers, Ju 287 (1944)
b) Hamburger Flugzeugbau, HFB 320 (1964)

2. Aspect-Ratio and Induced Drag

2.1 Vortex System Behind a Wing

The lift of a wing of finite span results from the pressure difference between the higher pressure on the wing's lower surface and the lower pressure on the wing's upper surface. As these pressures equalize at the wing tips, very strong free vortices develop behind the wing. Fig. 3 shows this effect with an airplane flying over a forest and emitting dust.

Figure 3 An airplane flying over a forest and emitting dust, [2, fig. 26]

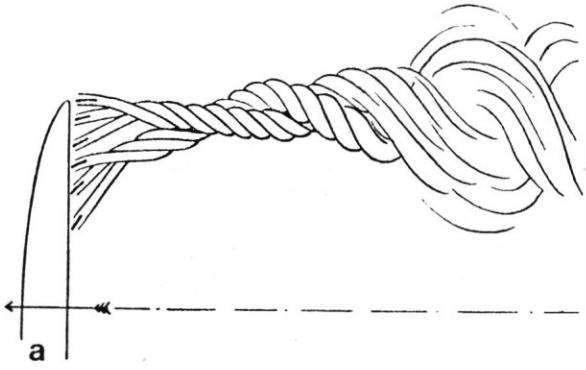

Figure 4 Vortex system behind a lifting wing
a) Lanchester's drawing of the vortex system around a wing (1907)
b) rolled-up vortex sheet (schematic)

This characteristic has been discovered by F.W. Lanchester [6] as early as 1907. He made the sketch of the boundary vortex reproduced in fig. 4a. The rolled-up vortex system behind a wing is again represented in fig. 4b. The energy required for the development of the vortex system behind the wing is the cause for the induced drag. It depends to a high degree on the wing aspect-ratio.

2.2 Prandtl's Theory of the Lifting Wing

The evaluation of induced drag D_i of simple unswept and untwisted wings was achieved by L. Prandtl in 1918 [8]. His theory does not take into account the complex rolling-up process of the free vortex sheet, as shown in fig. 4b. Assuming an elliptic distribution of circulation in the spanwise direction, there is a simple relation between the coefficient of induced drag c_{Di} and the lift coefficient c_L

$$c_{Di} = \frac{c_L^2}{\pi A} \sim \frac{1}{A} \quad \text{(Prandtl)}. \qquad (1)$$

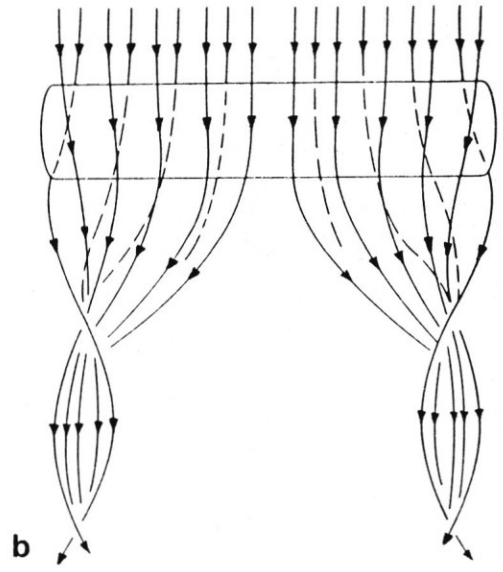

The excellent agreement between theory and experiment is demonstrated in fig. 5. Fig. 5a shows the drag polars $c_D = f(c_L)$ for different wings with aspect-ratios A = 1 up to A = 7, whereas fig. 5b presents the drag coefficients transformed to aspect-ratio A = 5 according to the theory.

2.3 Induced Drag for Arbitrary Wing Plan Form and Twist

The induced drag of wings depends within the linear theory only on the distribution of circulation in the spanwise direction. It is of no consequence in which way the distribution of circulation is produced by wing plan-form and twist. Major contributions to this subject for the non-rolled-up free vortex sheet have been made by L. Prandtl [8], M. Munk [7], K. Kraemer [5] and W.R. Sears [12]. W. Kaufmann [3] confirms the validity of Prandtl's theory for induced drag by taking into account the rolled-up free vortex sheet, see [13].

In fig. 6 the coefficient of induced drag according to eq. (1) is represented in logarithmic scale. To give an idea of the order of the aspect-ratios a few values of well-known aircraft are given. One can see that the aspect-ratios vary over a large range. The Mü 27 and SB 10 aircraft are gliders, which were constructed by Academic Flight Groups of the Technical Universities of Munich and Brunswick.

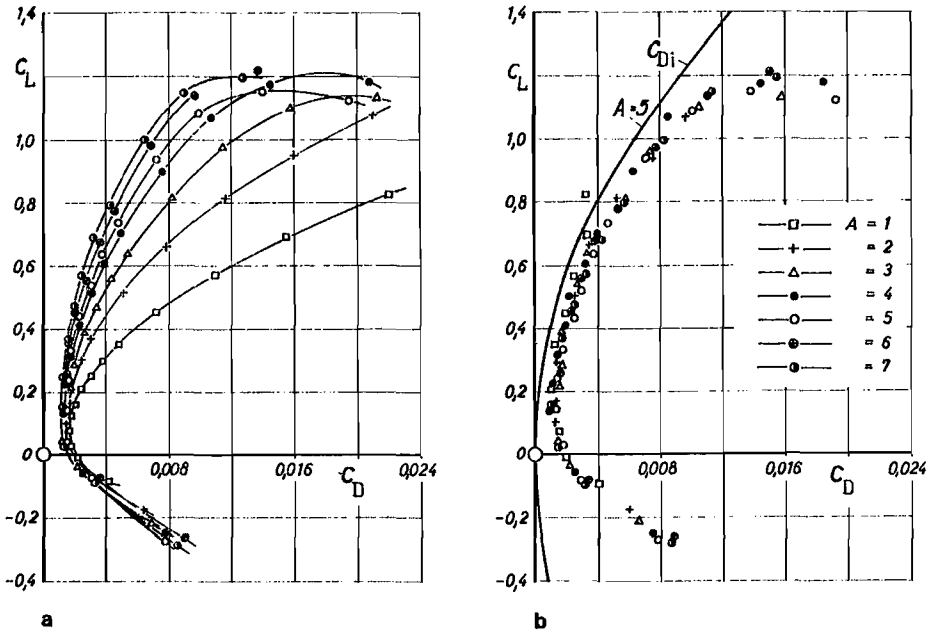

Figure 5 The drag of wings after Prandtl's lifting wing theory; demonstration of the experimental verification (1918)

a) polar curves for rectangular wings of aspect ratio $1 \leq A \leq 7$

b) polar curves transformed to A = 5

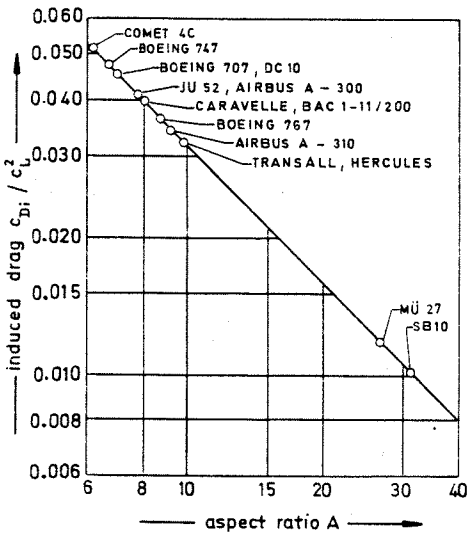

Figure 6 Induced drag as function of aspect-ratio (elliptic distribution of circulation); "o": values of aspect-ratios for some well-known airplanes

3. Twist and Induced Drag

3.1 Form of Wing Twist

The total twist of a wing section is made up of geometric, aerodynamic and elastic twist. Geometric twist is the torsion of the chord line against a wing reference plane. An aerodynamic twist results for cambered profiles and flaps. In such a case the local angle of incidence has to be measured from the no-lift direction.

Usually the wing structure is elastic. If the conventional wing after fig. 7a and b bends normal to the flectural axis then the swept-forward wing is subject to a positive twist with an additional loading at the outer part of the wing and the swept-back wing is subject to a negative twist with a corresponding lower loading. The forward sweep causes an unstable pitching moment due to elasticity. This structural instability is called aeroelastic divergence. As the degree of sweep increases, instability becomes more pronounced. To overcome this, an increasingly stiff and therefore heavy wing is needed. Composite structures could overcome divergence of conventional swept-forward wings. By varying the direction of the carbon-fibre plies in the wing skins and the thickness of those skins, it is possible to control the direction of the flexural axis and therefore the twisting of the wing under load. It is now possible to reverse the natural tendency of a swept-forward wing towards increased angle of incidence. The configuration becomes stable. By

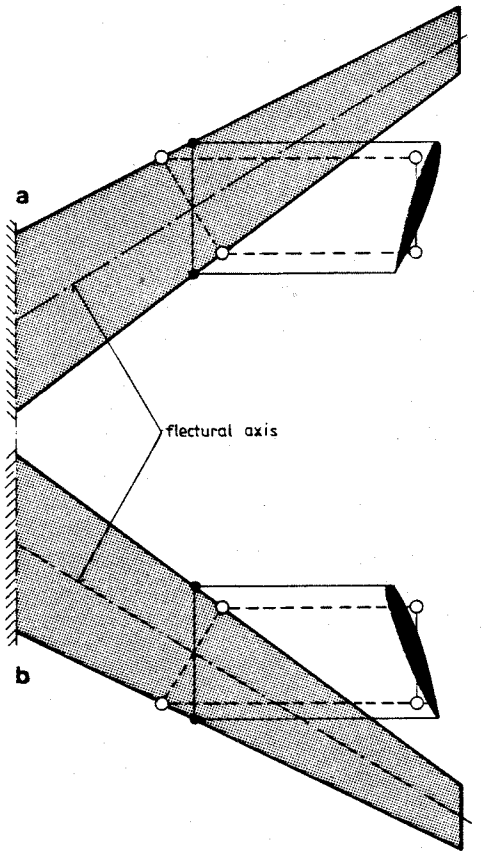

Figure 7 Elastic twist of conventional wings
a) swept-forward wing
b) swept-back wing

using composites the weight penalty for increased forward-sweep is minimal. For further details see [14].

In a program supported by the US Airforce, the NASA and the Defense Advanced Research Projects Agency (DARPA) an aircraft with a forward-swept wing is at present being investigated by Rockwell, Grumman and General Dynamics. Fig. 8 shows the project of Grumman.

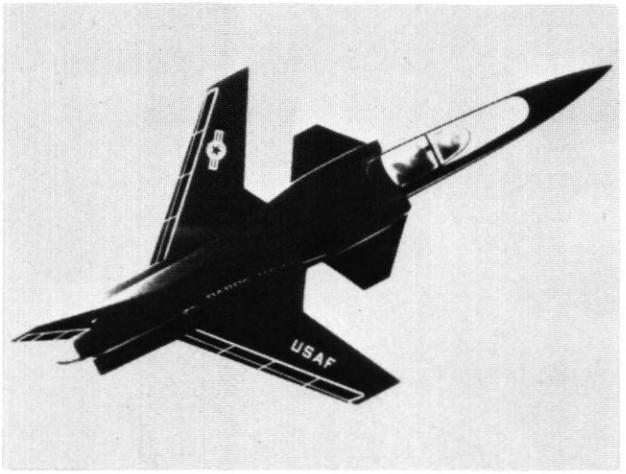

Figure 8 Project of a modern aircraft with swept-forward wing; Grumman (1979)

The advantage of a large aspect-ratio with respect to induced drag can be used in the case of several aircraft flying in a close formation or likewise in the case of birds on their long distant flights. The drag reduction in formation flight has been investigated theoretically by C. Wieselsberger, H. Schlichting and D. Hummel [1]. Fig. 9 shows some crane birds on their flight to Africa. Whereas the single bird has an aspect-ratio of $A \approx 3$, the formation allows an effective aspect-ratio of $A' \approx 20$. As every bird takes advantage in some way of the upwash of its fellow-birds, the birds in formation move at different angles of incidence while keeping their lift coefficient constant. This is similar to a twisted wing having constant local lift coefficient in spanwise direction. The distribution of twist angle depends whether the wing is swept back or forward.

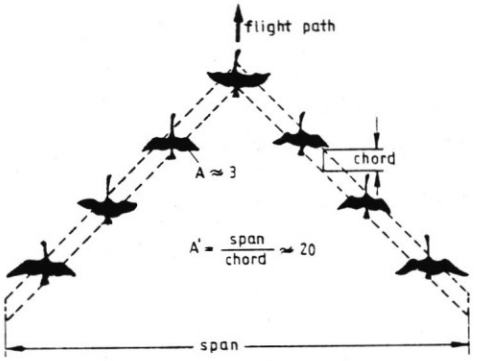

Figure 9 Flight of birds in formation (swept wing) to obtain a larger effective aspect-ratio

3.2 Determination of Induced Drag

Once the spanwise distribution of circulation $\Gamma(y)$ has been calculated for a given wing, see fig. 10, one finds the coefficient of induced drag

$$c_{Di} = A \int_{-1}^{1} \gamma(\eta)\alpha_i(\eta)\,d\eta \qquad (2a)$$

with the induced angle of incidence

$$\alpha_i(\eta) = \frac{1}{2\pi} \lim_{\varepsilon \to 0} \left[\frac{2}{\varepsilon}\gamma(\eta) - \int_{-1}^{1} \frac{\gamma'(\eta')\,d\eta'}{(\eta-\eta')^2} \right]. \qquad (2b)$$

In eq. (2a,b) $\gamma = \Gamma / b\,V$ is the distribution of circulation made dimensionsless by span b and air speed V, and $\eta = y/s$ is the spanwise coordinate related to semi-span $s = b/2$. First one determines from eq. (2a,b) the coefficient of induced drag at incompressible flow. The influence of Mach-number ($0 \leq Ma < 1$) can be obtained by means of the Prandtl-

Glauert-Goethert rule. The flow is transformed to an incompressible reference flow (Ma = 0, index "ic") for any subsonic Mach-number (Ma < 1). The parameters of the wing plan form are transformed as follows [11, chap. 4.4]:

$$\lambda_{ic} = \lambda \,, \quad \cot\Lambda_{ic} = \beta \cot\Lambda, \; A_{ic} = \beta A \qquad (3a)$$

where $\beta = \sqrt{1-Ma^2} < 1$. For the dimensionless distribution of circulation the following transformation applies:

$$\gamma(\eta) = \gamma_{ic}(\eta_{ic}) \,, \quad (\eta = \eta_{ic} \,, \; \alpha = \alpha_{ic}) \,. \qquad (3b)$$

The circulation distribution of a twisted wing may be represented by superposition of the distribution of the wing without twist γ_u and the distribution of the twisted wing γ_o for which the total lift is zero. Consequently the distribution of the circulation and the induced angle of incidence are given by

$$\gamma = \gamma_u + \gamma_o \,, \quad \alpha_i = \alpha_{iu} + \alpha_{io} \,. \qquad (4a,b)$$

Thus eq. (2a,b) for the induced drag of the twisted wing leads to [11, chap. 3.4.2]:

$$c_{Di} = c_2 \frac{c_L^2}{\pi A} + c_1 \, c_L + c_o \,. \qquad (5a)$$

If the wing has no twist, the induced drag is determined just by the term $c_2 \geq 1$. The wing with twist requires, in addition to this term, a term $c_1 \lesseqgtr 0$ that is proportional to c_L, and a term $c_o > 0$ that is independent of c_L. For the wing without twist, the factor c_2 represents the ratio of the induced drag to its minimum value for elliptic circulation distribution

$$(c_{Di})_{min} = \frac{c_L^2}{\pi A} \qquad (0 \leq Ma < 1) \qquad (5b)$$

It has to be pointed out that eq. (5b) is valid for the whole Mach-number range.

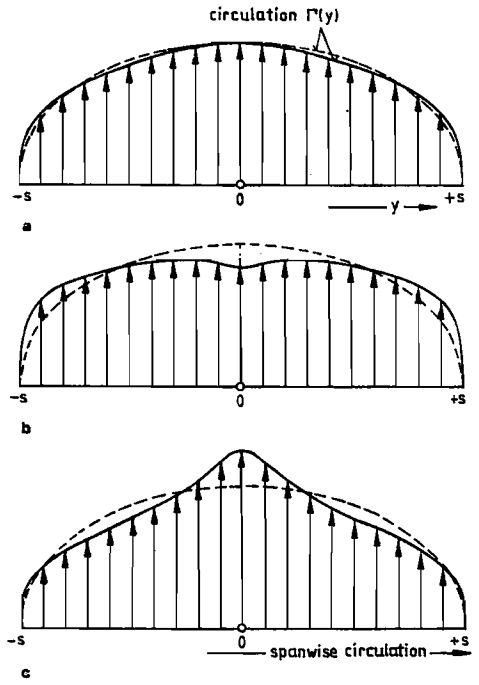

Figure 10 Spanwise distribution of circulation for untwisted wings (λ = 0,5; A = 9,0) at Mach-Number Ma = 0,1
a) wing without sweep, Λ = 0
b) swept-back wing, Λ = + 45°
c) swept-forward wing, Λ = -45°

3.3 Distribution of Circulation and Lift in Spanwise Direction +

For untwisted wings with a taper-ratio λ = 0,5 and an aspect-ratio A = 9,0, the spanwise circulation distribution $\Gamma(y)$

+ I am very much indepted to P. Sacher (Messerschmitt-Bölkow-Blohm, MBB) and to H. Brust (Institute of Fluidmechanics, Technical University Munich) for their help in calculating and evaluating the numerical results.

is represented in fig. 10a,b,c for three different sweeps $\Lambda = 0$, $= +45^{\circ}$, $= -45^{\circ}$ at Mach-number Ma = 0,1. The elliptic circulation distribution providing the same total lift is also represented. The circulation is higher at the outboard sections of the swept-back wing and higher at the inboard sections of the swept-forward wing.

The distribution of local lift coefficients $c_l(\eta)$ follows from the distribution of circulation $\gamma(\eta) = \Gamma(\eta)/b\,V = c_l(\eta)\, c(\eta)/2\, b$ with the local chord $c(\eta)$:

$$c_l(\eta) = \frac{2\,b}{c(\eta)}\,\gamma(\eta) = 2\,A\,\frac{c_m}{c(\eta)}\,\gamma(\eta). \quad (6a)$$

In this equation $A = b/c_m$ is the aspect-ratio. The local chord for tapered wings is given by

$$\frac{c(\eta)}{c_m} = 2\,\frac{1 - (1-\lambda)\eta}{1+\lambda} \qquad (0 \le \eta \le 1). \quad (6b)$$

Fig. 11 shows the spanwise distribution of local lift coefficient $c_l(\eta)$ for the three untwisted wings of fig. 10 with the total lift coefficient $c_L = 1{,}0$. The maximum local lift coefficients are marked by circles. They are located for the swept-back wing in the vicinity of the tips and for the swept-forward wing at the center of the wing. This remarkable effect of sweep is of major interest for the discussion of the characteristics of flow separation of swept wings at high angles of incidence.

In addition to this sweep effect caused by the spanwise lift distribution, swept wings are moreover subject to the influence of a boundary-layer effect on flow separation. Due to the sweep a pressure gradient on the upper surface of the wing causes a flow of the boundary layer in lateral direction. This leads to the consequence that the local maximum lift coefficients are limited.

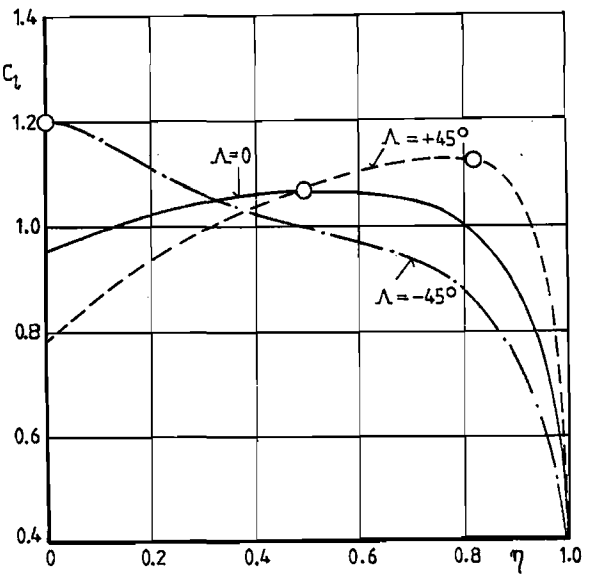

a

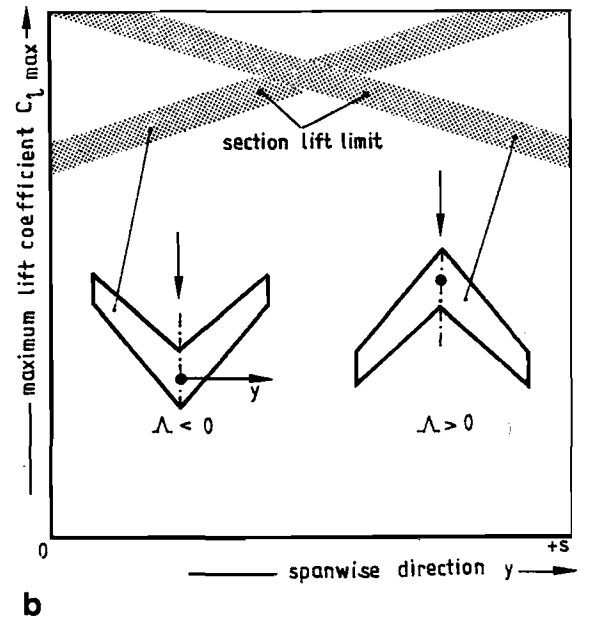

b

Figure 11 Spanwise local lift distribution at high angles of incidence
a) effect of sweep, untwisted wing (λ = 0,5; A = 9,0; $\Lambda = 0$, $= -45^{\circ}$, $= +45^{\circ}$), c_L = 1,0
b) effect of boundary layer, section lift limit for swept-back and swept-forward wings (schematic)

Fig. 11b represents schematically the section lift limit in dependence on the spanwise direction for the swept-back and for the swept-forward wing. The section lift limit depends not only on the sign of sweep (swept-back or swept-forward), but also on the stalling characteristics of the airfoil and on the presence of the fuselage.

Both the sweep-effect and the boundary-layer effect work in the same way causing the flow separation at high angles of incidence for swept-back wing at the tips and for the swept-forward wing at the center. The statements made above are confirmed by measurements. Fig. 12a,b shows the lift coefficient versus the angle of incidence for a swept-back wing and a swept-forward wing.

By wing twist an elliptic spanwise distribution of circulation can be obtained for a given design lift coefficient. The following results are based on a design lift coefficient $\bar{c}_L = 0{,}45$. This flight condition corresponds for piston engine aircraft approximately to an optimal value for c_L/c_D with c_D as coefficient for total drag and for jet engine aircraft to an optimal value for $Ma(c_L/c_D)$ with Ma as flight-Mach-number. The distribution of the circulation is equivalent to the load distribution in the spanwise direction. According to eq. (5b) the minimum induced drag for a given aspect-ratio A and wing lift coefficient c_L is obtained by an elliptic load distribution. Other load distributions are discussed in [4].

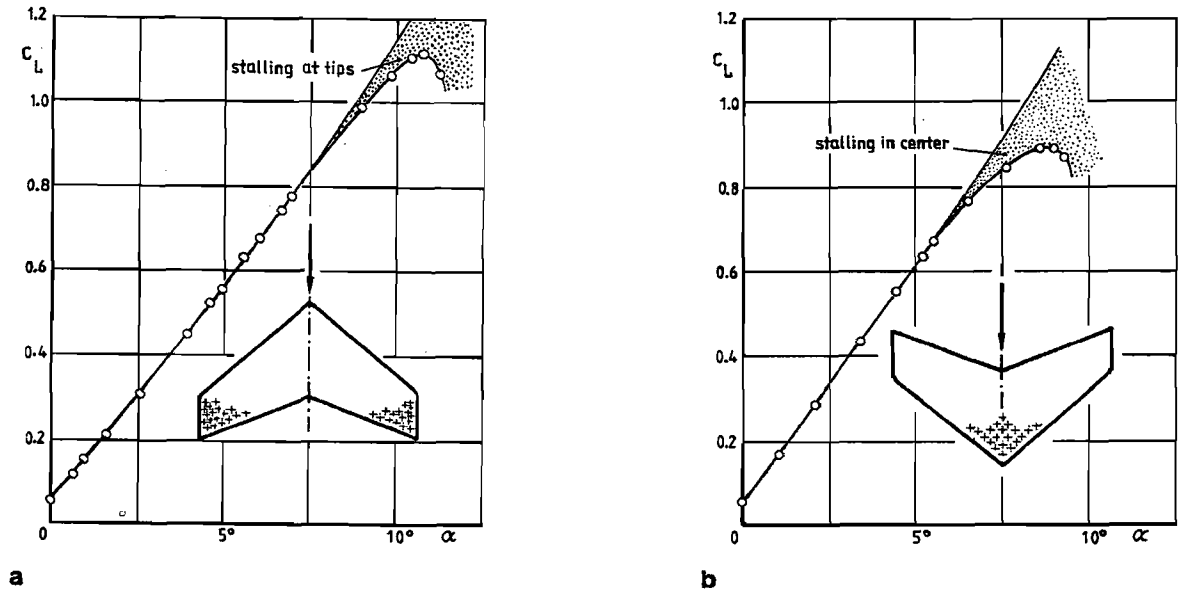

Figure 12 Lift coefficients for untwisted wings at high angles of incidence, development of the boundary layer

a) swept-back wing, boundary-layer displacement outboard the wing

b) swept-forward wing, boundary-layer displacement inboard the wing

Fig. 13a shows the distributions of spanwise lift coefficients at the high lift coefficient (c_L = 1,0) for the twisted wings having elliptic load distributions at the design lift coefficient ($\bar{c}_L$ = 0,45). Fig. 13b demonstrates the different onset of flow separation as a consequence of the above described sweep effect and boundary-layer effect. For the section lift limit the following relations have been used:

$$c_l = 1,3 - 0,2\eta \quad \text{for } \Lambda = +45^\circ \qquad (7a)$$

$$c_l = 1,1 + 0,2\eta \quad \text{for } \Lambda = -45^\circ. \qquad (7b)$$

The flow around a swept-back wing will stall first outboard, resulting in serious deterioration of the efficiency of the ailerons and a possible loss of lateral control. The opposite happens in the case of a swept-forward wing, with the flow separating inboard. The ailerons remain effective at high angles of incidence.

So far results were obtained for swept-back wings with a taper-ratio λ = 0,5. Since the taper-ratio has a strong influence on the spanwise load distribution other taper-ratios than λ = 0,5 have been investigated, see fig. 14a to d. Curve (1) describes the distribution of spanwise lift coefficient for the twisted wing at high lift coefficient ($c_L \approx 1,0$) having elliptic load distribution at the design lift coefficient ($\bar{c}_L$ = 0,45). The straight line labeled (2) according to eq. (7a) for the section lift limit is also represented. The points where flow separates first are marked by η^*. The more tapered the wing, the more the point of separation moves to the wing tips. By twisting the inboard area of the wing ($0 \leq \eta \leq \eta^*$) the flow separation can be shifted inboard. The twist should be made in such a way that the spanwise lift distribution follow the section lift limit in the range of $0 \leq \eta \leq \eta^*$

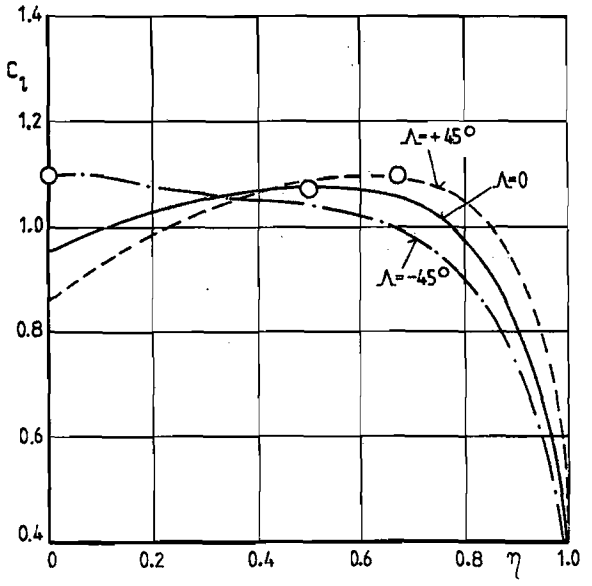

a

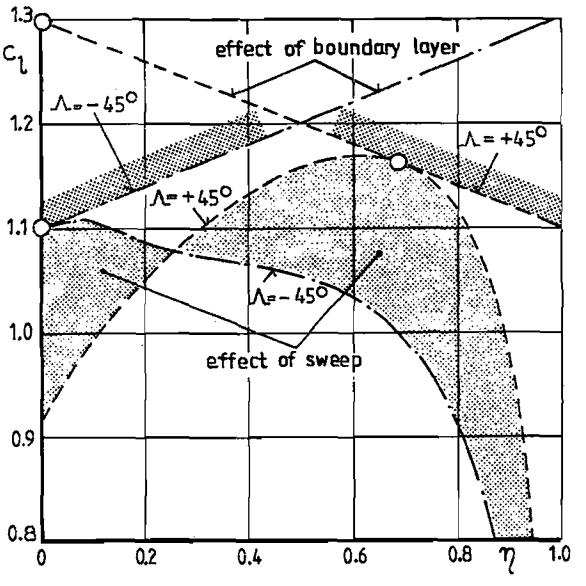

b

Figure 13 Spanwise local lift distribution for twisted wings (λ = 0,5; A = 9,0, Λ = 0, = - 45°, = + 45°; elliptic load distribution at design lift coefficient $\bar{c}_L$ = 0,45)

a) effect of sweep, c_L = 1,0

b) effect of sweep and boundary layer

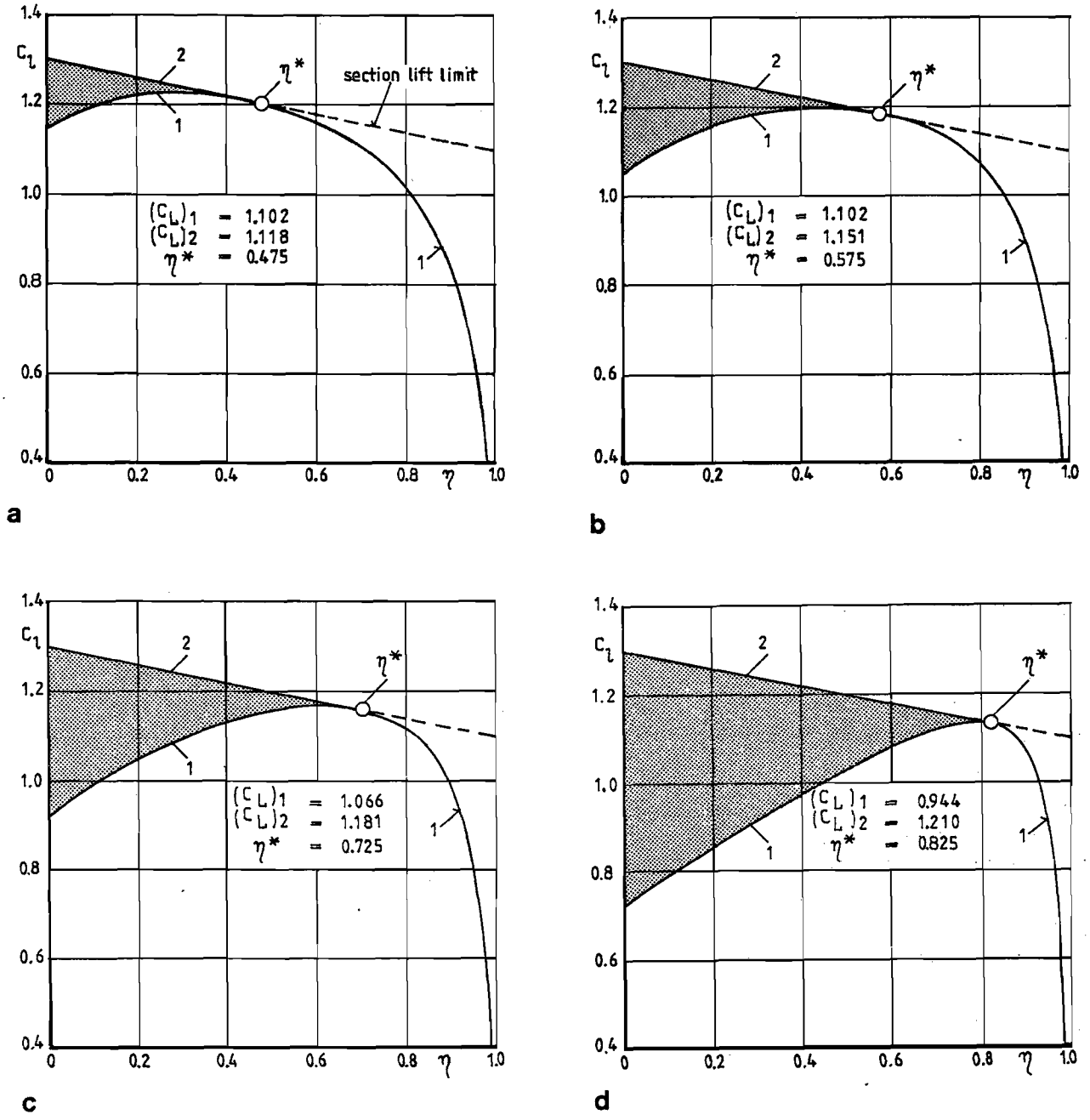

Figure 14 Spanwise local lift distribution for swept-back wings (A = 9,0; Λ = + 45°) for different taper-ratios λ in the vicinity of stalling ($c_L \approx 1,0$, Ma = 0,1)
a) λ = 1,0; b) λ = 0,75; c) λ = 0,5; d) λ = 0,25
curve 1: twisted wing (elliptic load distribution at design lift coefficient $\bar{c}_L$ = 0,45)
curve 2: twisted wing (linear decreasing lift coefficient inboard the wing, reaching the local maximum lift coefficient)

and remain unchanged with respect to curve (1) in the range of $\eta^* \leq \eta \leq 1$. Wings having such a spanwise lift distribution can be considered to have favourable stall characteristics.

As in the case of swept-forward wings flow separation always occurs at the center of the wing, a similar study as for the swept-back wing is not necessary. Swept-forward wings which are twisted in such a way that they have elliptic load distributions at $\bar{c}_L = 0{,}45$ do not need additional twist in order to have favourable stall characteristics.

4. Conclusions

4.1 Maximum Lift Coefficient

If the swept-back wings are twisted in such a way that the flow separates in the inboard area of the wing according to curve (2) in fig. 14a to d the maximum lift coefficients will thus be more or less enlarged as compared to the values according to curve (1). The figures contain explicit values for the lift coefficients $(c_L)_2 > (c_L)_1$. They are plotted in fig. 15 versus the taper-ratio λ. The values $(c_L)_2$ do not depend very much on λ. The lift coefficients $(c_L)_1$ are also included in fig. 15. They vary considerably with the taper-ratio λ. In the case of swept-forward wings these lift coefficients $(c_L)_1$ are of the same order of magnitude as the lift coefficients $(c_L)_2$ in the case of swept-back wings.

4.2 Optimum Wing

Within this study a wing will be considered to be of optimum design if it fulfills the following two conditions:

(I) design lift coefficient ($\bar{c}_L = 0{,}45$), elliptic spanwise load distribution

(II) high lift coefficient ($c_L \approx 1{,}0$), flow separation always inboard.

The present investigation on the use of twist as a means of changing spanwise lift distribution showed that the swept-back wing does not fulfill both conditions whereas this is the case for the swept-forward wing. However, it has to be pointed out that by applying special measures on the flow around the wing tips, e.g. winglets, as well as boundary-layer control the results obtained above can be altered to some extent.

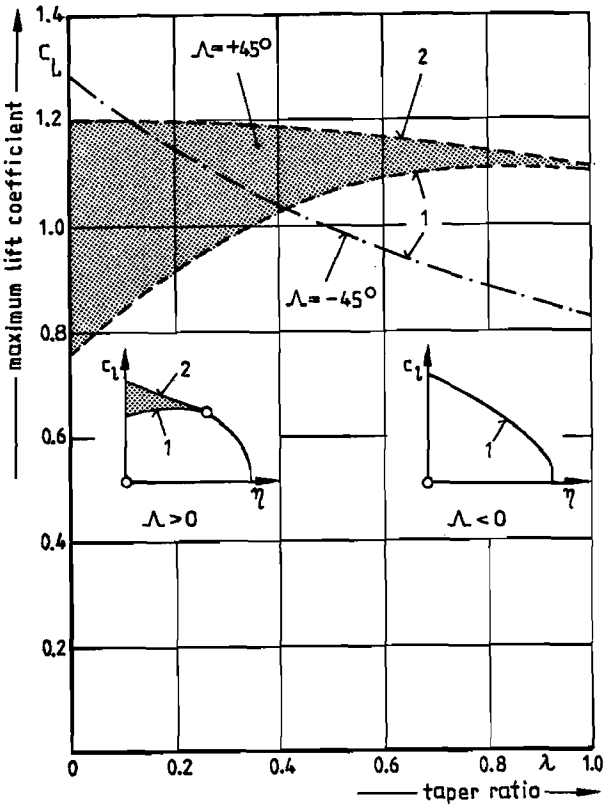

Figure 15 Maximum lift coefficients of swept wings (A = 9,0, $\Lambda = \mp 45°$) in dependence on taper-ratio λ
curve 1, curve 2: see fig. 14

4.3 Drag Polar

The twisted swept-forward wing has an elliptic load distribution at the design lift coefficient $\bar{c}_L = 0{,}45$. Hence it follows that such a wing with a given aspect-ratio A has the minimum coefficient for induced drag. For a twisted swept-back wing an elliptic load distribution at the design lift coefficient ($\bar{c}_L = 0{,}45$) cannot be achieved because of the requirement that the flow separates inboard for a high lift coefficient ($c_L \approx 1{,}0$). This means that this wing with a given aspect-ratio has a higher coefficient for induced drag than the minimum coefficient. Summing up the following is valid for $\bar{c}_L = 0{,}45$:

$$\bar{c}_{Di} = (c_{Di})_{min} = \frac{\bar{c}_L^2}{\pi A} \quad \text{for } \Lambda < 0 \qquad (8a)$$

$$\bar{c}_{Di} > (c_{Di})_{min} = \frac{\bar{c}_L^2}{\pi A} \quad \text{for } \Lambda > 0 \; . \qquad (8b)$$

For A = 9,0 the value of the minimum coefficient of induced drag is $(c_{Di})_{min} = 0{,}00716$.

The drag polars for swept wings with an aspect-ratio of A = 9,0 are plotted in fig. 16. The swept-forward wing fulfills both conditions (I) and (II) as formulated in section 4.2, whereas the swept-back wing only fulfills condition (II). One can see that in the case of swept-forward wings the taper-ratio nearly has no influence on the drag polar, and in the case of swept-back wings the polar drags deteriorate with decreasing taper-ratio. For comparison, the drag polar for elliptic load distribution is given by a dotted line.

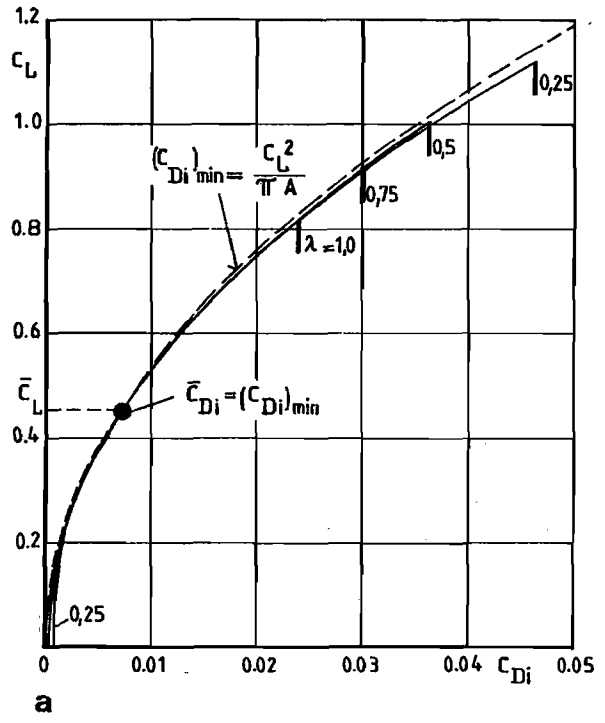

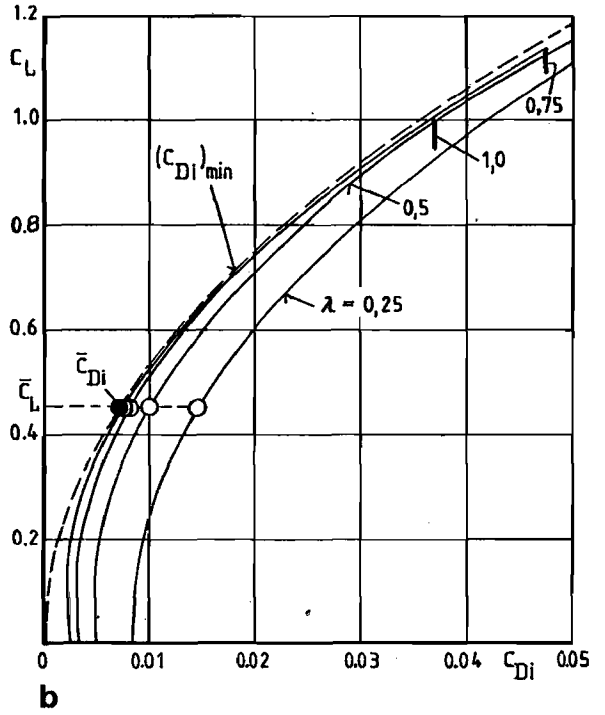

Figure 16 Drag polars for swept wings (A = 9,0; $\Lambda = \pm 45^o$; Ma = 0,1) at various taper-ratios ($0{,}25 \leq \lambda \leq 1{,}0$)
a) swept-forward wing: elliptic load distribution ($\bar{c}_L = 0{,}45$, $\bar{c}_{Di} = 0{,}00716$)
b) swept-back wing: local lift coefficient ($c_L \approx 1{,}0$), see fig. 14.

1	2	3	4		5	6	7
sweep Λ	aspect-ratio A	taper-ratio λ	condition (I)	(II)	$\frac{Di}{(D_i)_{min}}$	aspect-ratio A^*	$\frac{Di}{(D_i)_{min}}$
swept-forward ($\Lambda = -45^o$)	9,0	0,25			1,00	9,0	1,00
		0,50					
		0,75					
		1,00					
swept-back ($\Lambda = +45^o$)	9,0	0,25			2,00	18,7	1,00
		0,50			1,38	12,5	
		0,75			1,13	10,3	
		1,00			1,04	9,4	

Table 1 Geometric parameters of wings having the same induced drag at the design lift coefficient $\bar{c}_L = 0,45$

(I) elliptic load distribution ($\bar{c}_L = 0,45$)
(II) flow separation inboard ($c_L \approx 1,0$)

For the design lift coefficient ($\bar{c}_L = 0,45$) table 1 shows the drag characteristics (ratio of induced drag D_i to minimum induced drag $(D_i)_{min}$) of different tapered wings. The values for the swept wings at the same aspect-ratio A = 9,0 are listed in columns 2 and 5. For example, one can see that the swept-back wing with a taper-ratio $\lambda = 0,5$ has an induced drag which is 38% higher than the minimum induced drag which can be realized by swept-forward wings. The above mentioned results are plotted in fig. 17a.

If all wings should have the same minimum induced drag at the design lift coefficient ($\bar{c}_L = 0,45$, $\bar{c}_{Di} = 0,00716$) then the aspect-ratios for swept-forward wings remain unchanged A = 9,0. However, for swept-back wings the aspect-ratios must be increased, $A^* > 9,0$, see table 1 (columns 6 and 7). In order to determine the new value of the aspect-ratio A^* condition (II) concerning flow separation at high lift coefficients ($c_L \approx 1,0$) must be taken into account. For example, the original wing ($\lambda = 0,5$, $\Lambda = +45^o$, A = 9,0) has to be altered to the new wing ($\lambda = 0,5$, $\Lambda = +45^o$, $A^* = 12,5$). For all taper-ratios ($0,25 \leq \lambda \leq 1,0$) the results for the new aspect-ratios A^* are presented in the fig. 17b. The enlargement of aspect-ratio for swept-back wings is undesirable from the structural point of view.

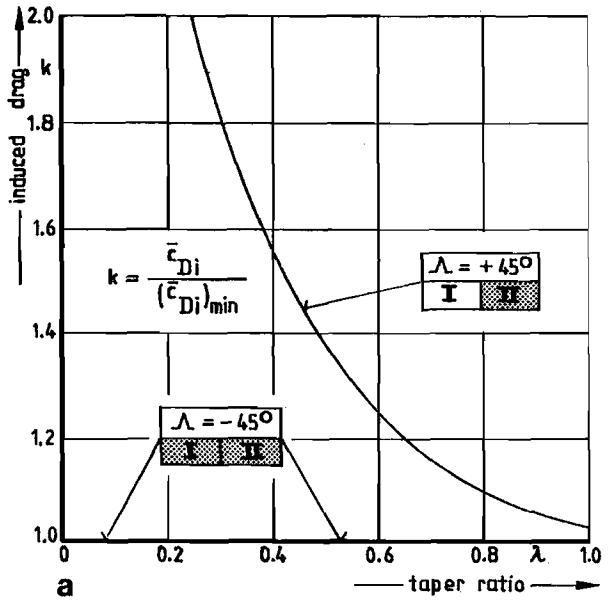

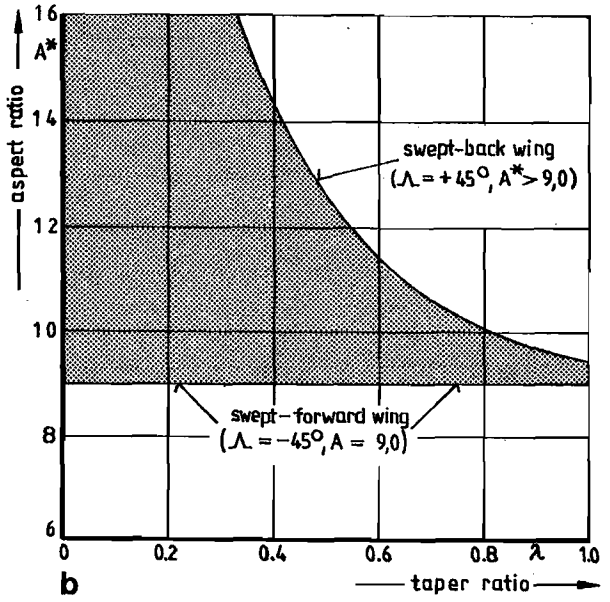

Figure 17 Influence of taper-ratio

a) ratio of induced drag to minimum induced drag at design lift coefficient for swept wings (A = 9,0, Λ = + 45°)

b) aspect-ratios for swept-back wings ($A^* > 9,0$, Λ = + 45°) having the same value of induced drag as the swept-forward wing (A = 9,0, Λ = - 45°)

In fig. 18 the drag polars for a swept-forward wing (λ = 0,5, Λ = - 45°, A = 9,0) and for a swept-back wing (λ = 0,5, Λ = + 45°, A^* = 12,5) are shown. At the design lift coefficient ($\bar{c}_L$ = 0,45) both have the same coefficient for induced drag ($\bar{c}_{Di}$ = 0,00716). The difference between the drag polars for lift coefficients other than the design lift coefficient stems from the different aspect-ratios A respectively A^*. All investigations are related to a flight Mach-number Ma = 0,1. By means of eq. (3a,b) the investigations can be extended to higher subsonic Mach-numbers.

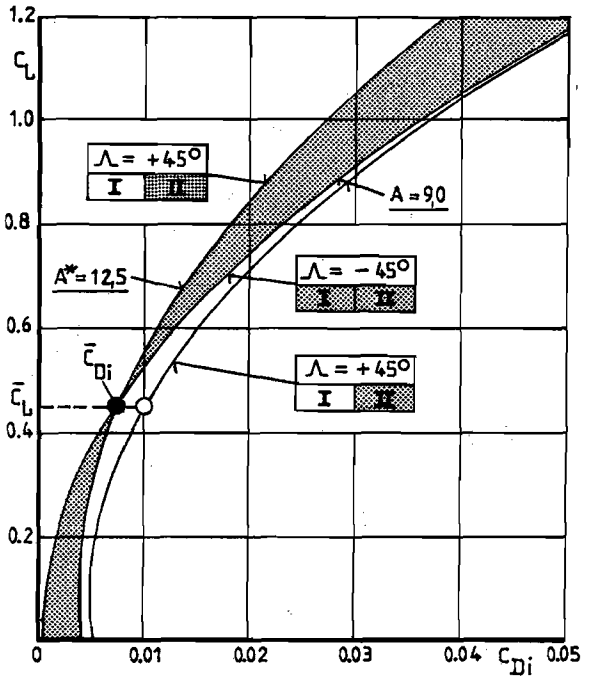

Figure 18 Comparison of drag polars of swept wings (λ = 0,5, Λ = - 45°, A = 9,0; λ = 0,5, Λ = + 45°, A^* = 12,5)

(I) elliptic load distribution ($\bar{c}_L$ = 0,45, $\bar{c}_{Di}$ = 0,00716)

(II) flow separation inboard ($c_L \approx 1,0$)

On the basis of a simple study a swept-forward wing with given aspect-ratio and a negative angle of sweep proves to be aerodynamically superior to a swept-back wing having the same aspect-ratio and the same, but positive angle of sweep. In other words for the same value of induced drag a swept-back wing should have a larger aspect-ratio than a swept-forward wing, both having the same, but opposite angle of sweep, see fig. 19.

A swept-forward wing combined with composite structure may provide - aside from individual performance benefit, for instance the effectiveness of the ailerons - a superior aircraft.

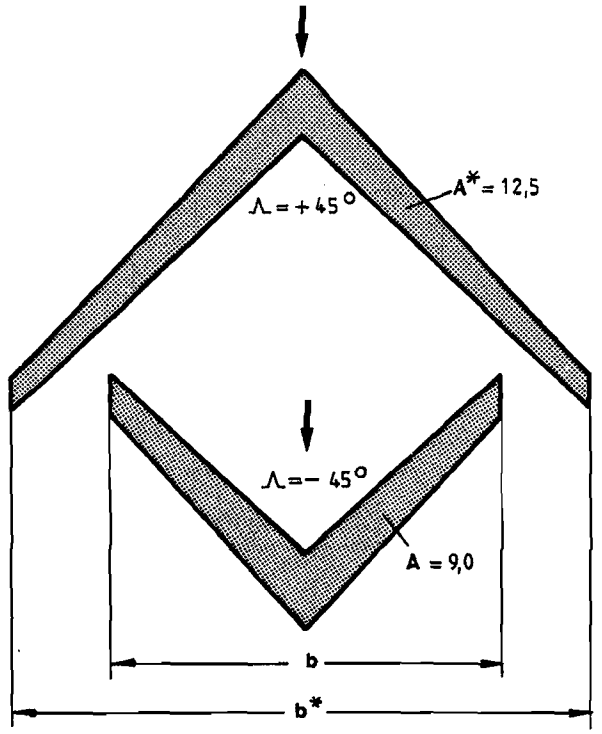

Figure 19 Comparison of swept wings with constant wing area having the same induced drag at the design lift coefficient ($\bar{c}_L$ = 0,45, $\bar{c}_{Di}$ = 0,00716) and having flow separation inboard at high lift coefficient ($\bar{c}_L \approx 1{,}0$)

swept-back wing: λ = 0,5; Λ = + 45°, A^* = 12,5

swept-forward wing: λ = 0,5; Λ = - 45°, A = 9,0.

References

(1) Hummel, D.:
Die Leistungsersparnis beim Verbandsflug. Journ. f. Ornithologie 114 (1973) 259-282; 119 (1978) 51-73
Comp.: Schlichting, H.: Jb. 1942/43 Dtsch. Akad. Luftfahrtforsch.; Wieselsberger, C.: Z.Flugtechn. Motorluftschiff. 5 (1914) 225-229

(2) Kármán, Th. von:
Aerodynamics, Selected topics in the light of their historical development. Ithaca (N.Y.): Cornell Uni. Press

(3) Kaufmann, W.:
Die energetische Berechnung des induzierten Widerstandes. Ing.-Arch. 17 (1949) 187-192; 18 (1950) 139-140

(4) Klein, A., Viswanathan, S.P.:
Approximate solution for minimum induced drag of wings with given structural weight. J. Aircraft 12 (1975) 124-126
Comp.: Prandtl, L.: Z. Flugtechn. Motorluftschiff. 24 (1933) 305-306 (reprinted Ges. Abh. 556-561 Berlin: Springer

(5) Kraemer, K.:
Über die Bewegungsgröße in der Trefftz-Ebene der Tragflügeltheorie und in sonstigen ebenen, inkompressiblen Potentialströmungen. Z. angew. Math. Mech. 18 (1968) 193-202
Comp.: AVA-Report 64 A 46 (1964)

(6) Lanchester, F.W.:
Aerodynamics and Aerodonetics. London: Constable, 1907/08

(7) Munk, M.M.:
Isoperimetrische Aufgaben aus der Theorie des Fluges. Dissertation Göttingen, 1919

(8) Prandtl, L.:
Tragflügeltheorie, I./II. Mitt. Nachrichten Ges. Wiss. Göttingen. Math. Phys. Klasse (1918) 451-477; (1919) 107-137 (reprinted Ges. Abh. 322-372, Berlin: Springer, 1961)

(9) Prandtl, L., Wieselsberger, C.:
Experimentelle Prüfung der Umrechnungsformeln. Erg. Aerodyn. Versuchsanst. Göttingen (AVA); I. Lief. (1920) 50-53

(10) Quick, A.W.:
Einige neuere Forschungsergebnisse auf dem Gebiet der Strömungen mit Energiezufuhr. Jb. 1968 Dtsch. Ges. Luft- u. Raumfahrt, 63-77

(11) Schlichting, H.; Truckenbrodt, E.:
Aerodynamics of the airplane.
New York: McGraw-Hill, 1979

(12) Sears, W.R.:
On calculation of induced drag and conditions down-stream of a lifting wing. J.Aircraft 11 (1974) 191-192

(13) Truckenbrodt, E.:
Die entscheidenden Erkenntnisse über den Widerstand von Tragflügeln. Jb. 1966 Wiss.Ges.Luft- u.Raumfahrt, 54-66

(14) Warwick, G.:
Forward sweep; Rockwell's new broom. Flight International, 1979, 1660-1662

Comp.: Aviation Week & Space Technology,
June 1978, Jan., Sept.; Dec. 1979;
April, May, June 1980

(15) Weeks, T.; Uhuad,G.C.; Large,R.A.:
An investigation of the transonic aerodynamic characteristics of forward-swept wings. Jb. 1980 Dtsch.Ges.Luft-u. Raumfahrt (in print)